Bridge Monitoring by a Monostatic/Bistatic Interferometric Radar Able to Retrieve the Dynamic 3D Displacement Vector

IEEE Access
Multidisciplinary ⋮ Rapid Review ⋮ Open Access Journal

Received November 3, 2020, accepted November 17, 2020. Date of publication xxxx 00, 0000, date of current version xxxx 00, 0000.

Digital Object Identifier 10.1109/ACCESS.2020.3039381

Bridge Monitoring by a Monostatic/Bistatic Interferometric Radar Able to Retrieve the Dynamic 3D Displacement Vector

LAPO MICCINESI, (Member, IEEE), AND MASSIMILIANO PIERACCINI, (Member, IEEE)
Department of Information Engineering, University of Florence, 50139 Firenze, Italy

Corresponding author: Lapo Miccinesi (lapo.miccinesi@unifi.it)

This work was supported in part by the Cassa di Risparmio di Firenze Foundation, 2018 Grant, ID 24099, cod. SIME 2018.0972.

ABSTRACT A monostatic/bistatic radar for retrieving the three-dimensional (3D) displacement vector is proposed for static and dynamic monitoring of bridges. The radar is particularly suitable for dynamic test, as it is able to detect the three components at high sampling frequency (132 Hz, in the reported case study). The monostatic/bistatic technique makes use of a multiple input multiple output (MIMO) interferometric radar equipped with two transponders. Each single transponder consists of an antenna and an amplifier and it is connected to the radar with a radiofrequency (RF) cable. A simulation has preliminarily estimated the expected accuracy in terms of positing error of transponders. The equipment and the method were experimentally tested in a controlled scenario using a vertical steel bar as target. Finally, the method was applied on a real case of interest: the dynamic monitoring of a bridge (''Ponte Nuovo sull'Arno'' in Lastra a Signa, Firenze, Italy) excited by the vehicular traffic. The 3D displacement vector was detected in time and the modal frequencies of each component were estimated.

INDEX TERMS Bridge monitoring, interferometry, MIMO, monostatic/bistatic radar, vibration measurement.

I. INTRODUCTION

Since 2007 [1] the interferometric radar has been proposed as portable and easily deployable sensor for static and dynamic monitoring of bridges. In a typical installation, the radar is positioned under the deck and detects the displacement of scatter points on the bridge that is able to image. In an alternative configuration, the radar points out the stay cables of the bridge for detecting their modal frequencies [2]. In the last years, bridge monitoring by terrestrial interferometric radar has become quite a popular technique [3]–[6].

A terrestrial interferometric radar is able to detect only the component of the displacement of the deck along the range direction. This only information can be not enough when the vectorial direction of the deck displacement is not *a priori* known. Indeed, Dei *et al.* [7] experimentally showed how the detection of a single component can give the paradoxical result of a bridge deck that is apparently raised when loaded. This is the reason of the increasing interest in radar configurations able to retrieve more than a single component of the displacement.

In 2018 Monti-Guarnieri *et al.* [8] developed a technique for operating up to three radars simultaneously for detecting the displacement vector of corner reflectors fixed to a pipe. In 2020 Deng *et al.* [9] performed an experiment which involves the simultaneous deployment of three ground-based multiple-input multiple-output (GB-MIMO) radar systems to measure 3-D deformation of a movable corner reflector. Both these approaches are based on the deployment of two or more radar systems, with evident drawbacks in terms of cost and complexity of the installation.

In 2017 Pieraccini *et al.* [10] first proposed the use of a transponder instead of a second radar for detecting two components of the (static) displacement of a corner reflector. In 2019 [11] the same authors extended the technique to the detection of two components of the dynamic displacement of a slender structure. The main advantage of the bistatic technique using transponders is to reduce the cost and the installation complexity. Moreover, the signals of different channels are measured by the same equipment, without problems of synchronization, resampling, and phase calibration.

The associate editor coordinating the review of this manuscript and approving it for publication was Yiming Huo.

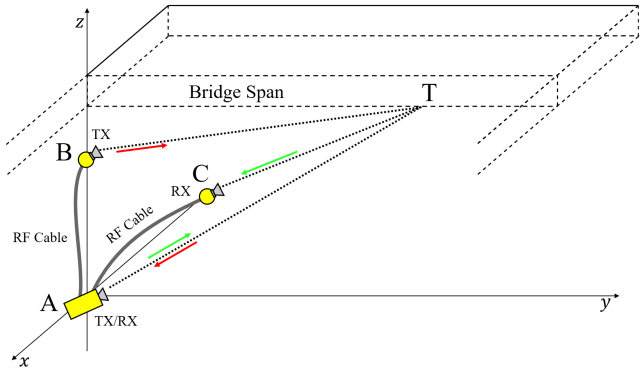

FIGURE 1. Measurement geometry of monostatic/bistatic radar technique applied to the dynamic monitoring of a bridge.

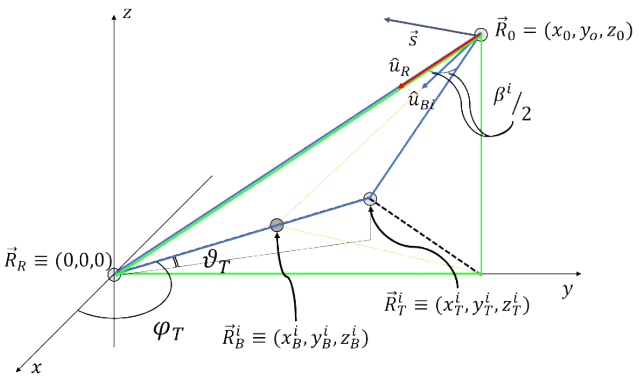

FIGURE 2. Bistatic geometry for retrieving the displacement vector.

The present paper extends, for the first time, the technique of transponders to the dynamic detection of all three components of the displacement.

Furthermore, the paper extends the bistatic technique to a complex structure: a real bridge instead of a tower. Indeed, a tower has the important advantage that can be considered an almost one-dimensional structure: this simplifies the identification of the radar target. The case of a bridge is rather more complex. Moreover, the uncertain related to the monostatic/bistatic technique was evaluated with a suitable simulation.

II. WORKING PRINCIPLE

Fig. 1 shows a sketch of the measurement geometry for detecting the dynamic 3D displacement of a bridge span using a single radar and two transponders.

The radar equipment was located under the bridge in the point A, close to the abutment. Two transponders were in the points B and C. Each transponder consists of an antenna, an amplifier and a radiofrequency (RF) cable.

The radar had two transmitting (TX) channels and two receiving (RX) channels. Two horn antennas fixed to the radar head provided the monostatic configuration. A TX channel was connected with an RF cable to the transponder B. So, the first bistatic path was radar - transponder B - target - radar (red arrows in Fig. 1). A RX channel was connected with an RF cable to the transponder C. So, the second bistatic path was radar - target - transponder C – radar (green arrows in Fig. 1).

The radar performs three measurements in fast sequence: monostatic acquisition (from A to A), first bistatic acquisition (from B to A), and second bistatic acquisition (from C to A).

Therefore, the radar detects the components of the displacement along range direction (by monostatic acquisition), along the bisector of the angle B-T-A, and along the bisector A-T-C. The bisector is different for any point target T.

The radar is able to perform a complete measurement cycle in 7.56 ms, so the displacement vector (for any point target of the bridge) can be retrieved in time with 132 Hz sampling frequency.

Fig. 2 depicts the bistatic configuration considering a single transponder i in a generic position $\vec{R}_T^i$. The radar is in $\vec{R}_R$ and can detect the displacement (ds_R) of a generic target ($\vec{R}_0$) by measuring the difference of the phase between two measurements ($\Delta\phi_R$):

$$ds_R = \frac{\lambda}{4\pi}\Delta\phi_R \tag{1}$$

where λ is the wavelength related to the central frequency.

With reference to Fig. 2, the bistatic angle (β^i) can be calculated as [10], [11]:

$$\beta^i = \cos^{-1}\left(\frac{\left|\vec{R}_{Ti} - \vec{R}_0\right| + \left|\vec{R}_0\right| - \left|\vec{R}_{Ti}\right|}{2\cdot\left|\vec{R}_{Ti} - \vec{R}_0\right|\left|\vec{R}_0\right|}\right) \tag{2}$$

The displacement along the bisector can be retrieved as:

$$ds_B^i = \frac{\lambda}{4\pi\cos\left(\frac{\beta^i}{2}\right)}\Delta\phi_{Bi} \tag{3}$$

The Cartesian components (dx, dy, dz) of the displacement can be retrieved by one monostatic displacement (ds_R) and two bistatic displacements (ds_{B1}, ds_{B2}) detected using the two transponders:

$$\begin{pmatrix} dx \\ dy \\ dz \end{pmatrix} = M^{-1}\begin{pmatrix} ds_R \\ ds_B^1 \\ ds_B^2 \end{pmatrix} \tag{4}$$

where ds_B^1, ds_B^2 are the displacement measured from different positions using (3) and M^{-1} is the inverse of the rotation matrix given by:

$$M = \begin{pmatrix} \hat{u}_R\cdot\hat{i} & \hat{u}_R\cdot\hat{j} & \hat{u}_R\cdot\hat{k} \\ \hat{u}_{B1}\cdot\hat{i} & \hat{u}_{B1}\cdot\hat{j} & \hat{u}_{B1}\cdot\hat{k} \\ \hat{u}_{B2}\cdot\hat{i} & \hat{u}_{B2}\cdot\hat{j} & \hat{u}_{B2}\cdot\hat{k} \end{pmatrix} \tag{5}$$

where $\hat{i}, \hat{j}, \hat{z}$ are the unit vector of coordinates axis and $\hat{u}_R$ and $\hat{u}_{Bi}$ are the unit vector shown in Fig. 2.

The unit vector can be retrieved considering the geometry in Fig. 2:

$$\hat{u}_R = \frac{\vec{R}_0 - \vec{R}_R}{\left|\vec{R}_0 - \vec{R}_R\right|} \tag{6}$$

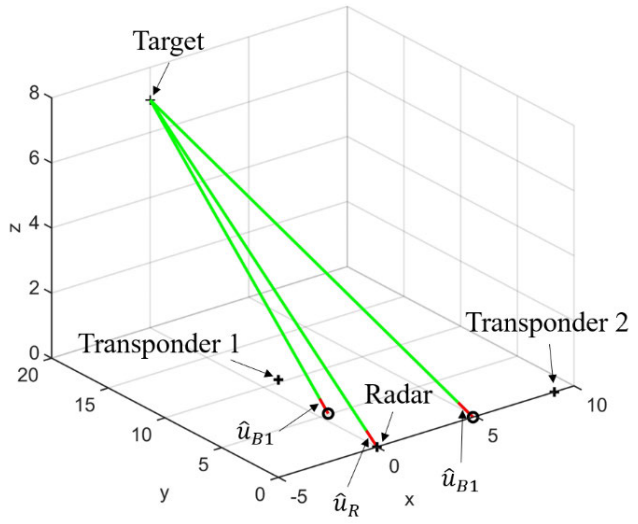

FIGURE 3. Simulation geometry.

$$\hat{u}_{Bi} = \frac{\vec{R}_0 - \vec{R}_B^i}{\left|\vec{R}_0 - \vec{R}_B^i\right|} \tag{7}$$

where $\vec{R}_B^i$ is the position of the bisector position of $\widehat{R_R R_0 R_T^i}$ angle. The magnitude of $\vec{R}_B^i$ can be found using the Carnot theorem:

$$\left|\vec{R}_B^i\right| = \frac{\left|\vec{R}_T^i - \vec{R}_0\right|^2}{\left|\vec{R}_T^i - \vec{R}_0\right|^2 + \left|\vec{R}_R - \vec{R}_0\right|^2} \left|\vec{R}_T^i - \vec{R}_R\right| \tag{8}$$

while its azimuth and elevation position are the same of the transponder.

III. UNCERTAIN ESTIMATION

The estimation of the displacement vector relies on the positions of the transponders, that have to be known. In order to evaluate the impact of the possible error in the positioning of the transponders, a simulation has been carried out.

The geometry of the simulation is shown in Fig. 3. The nominal position of radar, transponders and target are reported in Table 1. The nominal displacement of the target was (dx, dy, dz) = (0 mm, 0 mm, 0.5 mm). The length of cable between radar and transponder was 30 m.

In Fig. 3, the positions of bisectors are marked with **o**, the unit vectors $\hat{u}_R$ and $\hat{u}_{Bi}$ are represented with red lines.

The radar operates a continuous-wave step-frequency (CWSF) sweep with central frequency f_c= 17.20 GHz, bandwidth B = 800 MHz and number of frequencies N_f = 800.

The signal-to-noise (SNR) of the signal was supposed 15 dB. This value considers all possible error sources of radar. The positions of transponders were supposed have Gaussian uncertainty σ = 0.5 m. The simulation was run 1000 times. The average and standard deviation of displacement vector were calculated.

The results are reported in Table 2. The average values are in good accordance with the nominal values, and the standard deviations are comparable with the experimental uncertainty of a typical (monostatic) radar measurement, that is about 0.1 mm [12]. The simulation was also performed without positioning uncertain, i.e. using only the SNR. In this case the standard deviation (SD) was (SD_X, SD_Y, SD_z) = (0.0623, 0.0873, 0.2730) mm. So, we can affirm that the possible positioning error (not larger than 0.5 m) does not affect significantly the measurement, at least for the geometry in Fig. 3 that is rather similar to the geometry of the acquisition reported in the experimental section of this article.

TABLE 1. Position of Radar, transponders and target.

	Position (x, y, z) [m]
R_R	(0,0,0)
R_T^1	(-5,0,3)
R_T^2	(9,0,0)
R_0	(0,20,7)

TABLE 2. Position of Radar, transponders and target.

	Nominal displacement [mm]	Average displacement [mm]	Standard deviation [mm]
dx	0.0	0.0079	0.0694
dy	0.0	0.0021	0.0923
dz	0.5	0.4931	0.2858

FIGURE 4. Radar configuration with four antennas connected.

IV. RADAR EQUIPEMENT

The radar used is a modified version of IBIS-FM MIMO [13]. Fig. 4 shows IBIS-FM MIMO with the four antennas connected. The IBIS-FM MIMO provides a continuous-wave frequency-modulation (CWFM) signal with f_c= 17.2 GHz, B_{max}= 400 MHz. The radar has two TX channels and two RX channels. The acquisition frequency depends on the radar parameters (unambiguous range, range resolution, ...).

Fig. 4 shows the block scheme of the modified radar. The transponders were connected to the upper channel of the radar through RF cables of 28.82 m equivalent length and −30 dB attenuation. Two amplifiers (56 dB gain in transmission and

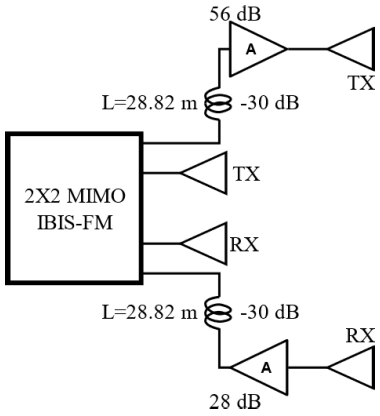

FIGURE 5. Block scheme of monostatic/bistatic radar.

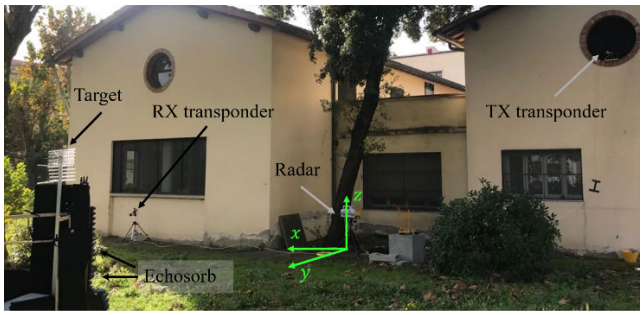

FIGURE 6. Radar installation in controlled scenario.

TABLE 3. Position of Radar and transponders.

	Position (x, y, z) [m]
R_R	(0,0,0)
R_{TX}	(-5.72, -2.73, 3.76)
R_{RX}	(6.66, 0.71, 0)
R_{Target}	(0, 6.73, 1.20)

28 dB in reception) compensate the cable-attenuation and increase the SNR.

In order to validate the method, the radar equipment was installed in a controlled scenario. The radar was in front of a vertical steel bar as Fig. 6 showed. The TX was located on a window at the second floor of the laboratory building. The RX transponder was located on the right of the radar. The coordinates of each of those are reported in Table 3.

The target was a steel bar with a metallic fence fixed on the top. Most of the bar was shielded by electromagnetic absorbers (Echosorb) as shown in Fig. 6. A seismic accelerometer, PCB 393B31 by PCB piezotronics, was fixed on of the bar. The accelerometer was oriented along the y-axis.

The measurement was performed along one axis for measuring and quantify the possible residual in the other axes.

Fig. 7 shows the three bistatic components measured by the radar and transponders between 0 and 5 s. The components of the movement can be retrieved by applying (3) and (4) to

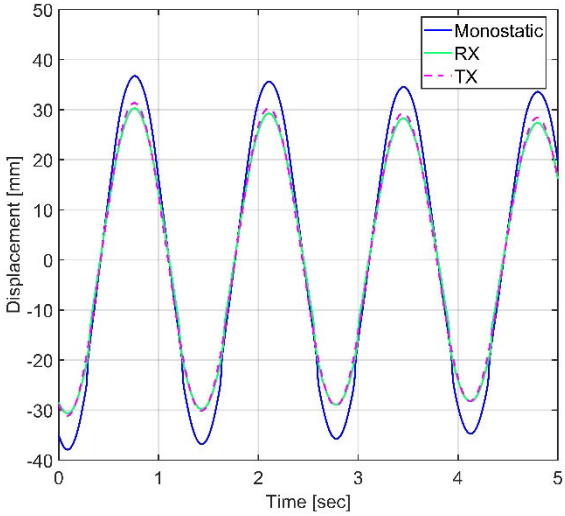

FIGURE 7. Displacement components of the steel bar measured by radar and transponders.

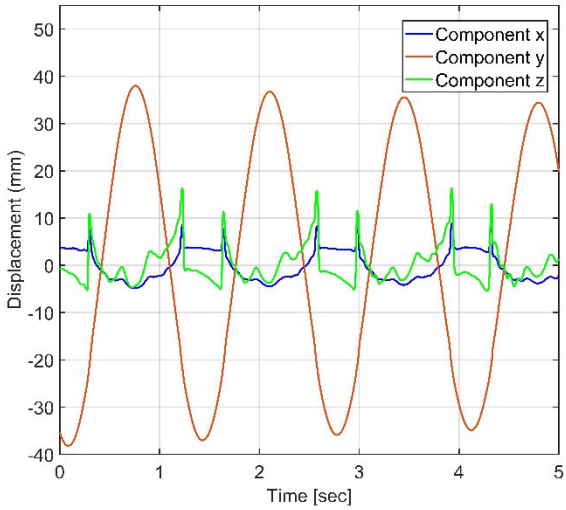

FIGURE 8. Displacement components of the steel bar.

the three signals in Fig. 7. The applied rotation matrix, M^{-1}, was:

$$M^{-1} = \begin{pmatrix} 1.6635 & -1.8835 & -0.1115 \\ 0.1103 & 0.4313 & 0.5958 \\ 5.3127 & -2.5346 & -3.5010 \end{pmatrix} \quad (9)$$

Fig. 8 shows the three components of displacement vector in Cartesian coordinates. The main displacement was along y-axis (as expected), even if we can note some displacement along the other axes. The component along z can be a residual or a ''pendulum'' effect. The component along x is probably given by misalignment of the target.

As further verification the radar and the accelerometer were compared. The result of the accelerometer was numerically integrated two times to obtain a displacement value. The two displacements, from the radar and accelerometer, were re-sampled with the same frequency and filtered with

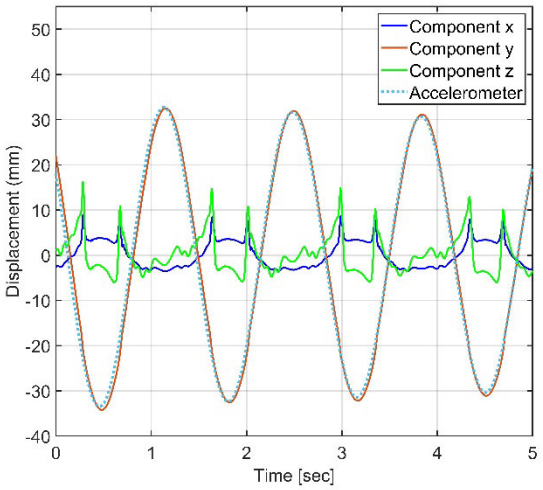

FIGURE 9. Comparison between radar and accelerometer.

a band pass filter between 0.5 Hz and 50 Hz. The result is shown in Fig. 9.

V. EXPERIMENTAL RESULTS

The monostatic/bistatic radar has been experimental tested on a bridge named ''Ponte Nuovo sull'Arno'', in Lastra a Signa, Firenze, Italy.

The ''Ponte Nuovo sull'Arno'', briefly Signa bridge, was rebuilt in 1948 near to the original location of the medieval bridge (1120 A.D.). The original bridge was destroyed during the World War II. The new bridge was built with reinforced concrete and it is composed by three spans over the Arno river and three spans over the embankment.

Fig. 10 shows the bridge and the radar installation. The radar was installed close to the embankment pillar. The TX transponder was fixed on the pillar above the radar. The RX transponder was located on the left side respect to the radar.

During the measurement campaign the bridge was opened to the traffic. The aim was just to detect the stress due to heavy vehicular traffic.

The coordinates of radar and transponders are reported in Table 4. The coordinates were measured using squares and meters, since the positioning error does not affect the measurement uncertain. Moreover, a total station or a more sophisticate method can be used for measuring the coordinates.

The x-axis was parallel to the pillar and corresponds to the transversal direction. The y-axis corresponds to the longitudinal direction of the bridge. The radar was located in the middle of the bridge.

Fig. 11 shows the radargram (amplitude plot) obtained by calculating the Fourier transform of the windowed echo (Kaiser window with $\beta = 5$). The peaks of the three channels do not correspond because of the different positions of antennas and the length of the RF cables.

With the aim to select the same scatter point in the three plots, the signals were focused on the bridge span along the median axe using a back-propagation algorithm [14],

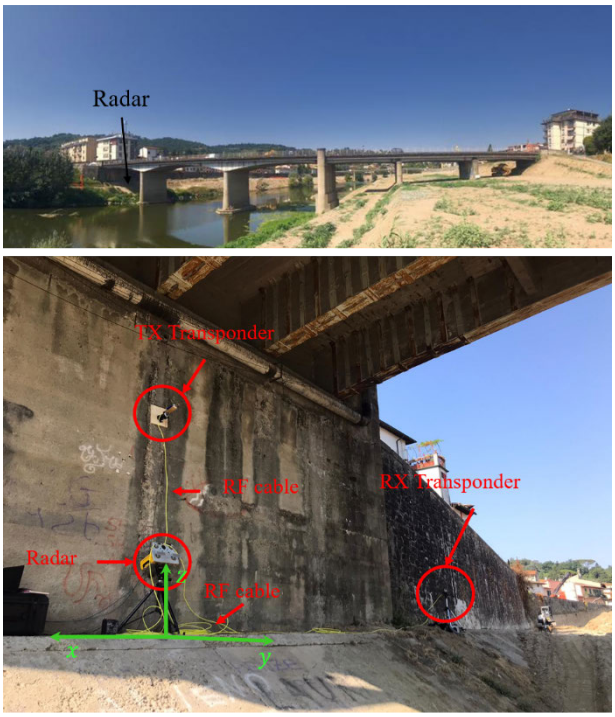

FIGURE 10. Signa bridge (upper picture) and radar installation (lower picture).

TABLE 4. Position of Radar and transponders.

	Position (x, y, z) [m]
R_R	(0, 0, 0)
R_{TX}	(0, 0, 3.06)
R_{RX}	(-8.72, 0, 0.1)
Height of the span	5.44

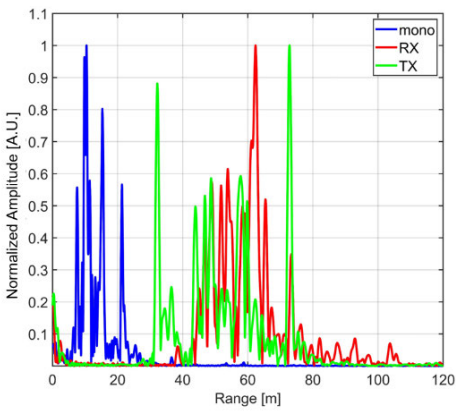

FIGURE 11. Radargrams relative to the three channels (the monostatic channel and the two bistatic channels).

by taking into account the positions of the radar, the transponders, the length of the RF cables and the height of the span.

The obtained plot is shown in Fig. 12. The signal at 20.60 m corresponds to the pillar of the bridge. The target

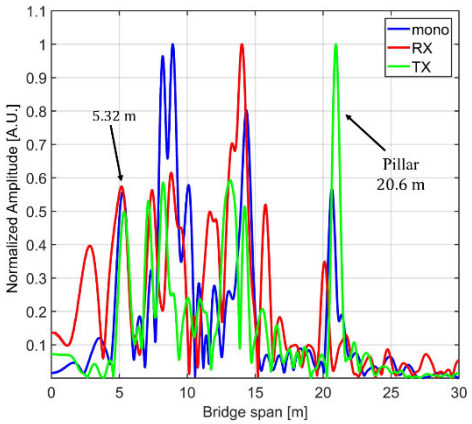

FIGURE 12. Radargram relative to the three channels focused on the bridge span.

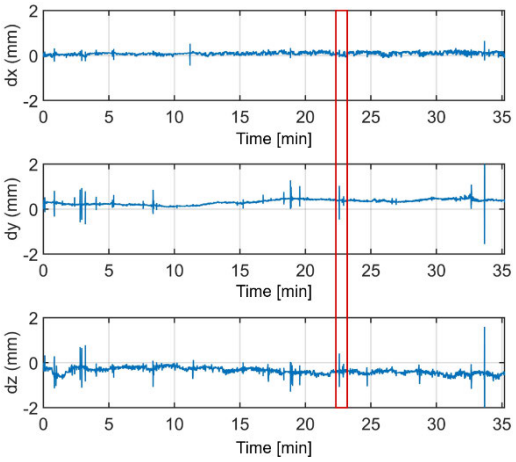

FIGURE 13. Displacement components of a target in the point of Cartesian coordinates (0.00 m, 5.32 m, 5.44 m).

used for bistatic analysis was marked in Fig. 12, it corresponds to the position (0.00 m, 5.32 m, 5.44 m). For this position, the displacement vector was evaluated using eq. (4).

Fig. 13 shows the three components of displacement. We can note some impulsive stimula, that involve simultaneously y and z axis. The pulses along x direction appears to be independent. For example, the red square spotlights a stimulus involved both z and y-axis. Fig. 14 shows a magnification of this area.

Fig. 14 shows two examples of two events. The event marked with A involved both z and y components, while the event marked with B involved only z component.

In order to determinate the preferential direction of the displacement, the whole measurement was visualized as scatter plot in the plane $x - z$ (Fig. 15 upper) and as scatter plot in the plane $y - z$ (Fig. 15 lower). The signals were filtered with a bandpass 0.1 Hz - 50 Hz for cutting off possible drift and high frequency noise.

It is interesting to note that in $x - z$ plane the main direction of displacement is vertical (as expected), but in $y - z$ direction there are two main directions: vertical and with

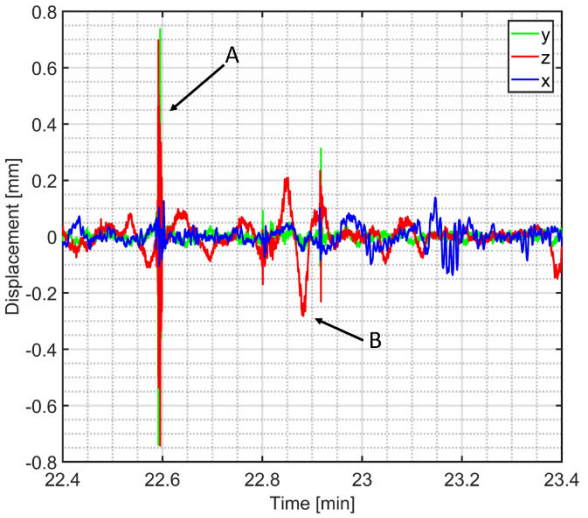

FIGURE 14. Magnification of Fig. 13. The event marked with A involved z and y components. The event marked with B only z component.

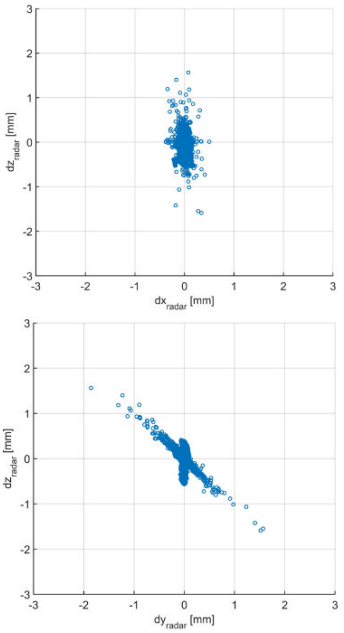

FIGURE 15. Scatter plots of the displacement on x-z plane (upper image) and on y-z plane (lower image).

an angle of 38.4°. Indeed, by observing the single stimula, we note that most of the impulses due to the vehicular traffic give vertical displacements, but sometimes we observe large impulses that exhibit this tilted direction of the displacement. We do not have a convincing explanation of this. However, we think it is somehow linked to the fact that there is a traffic light at the very beginning of the bridge and that cars sometimes have to stop and start on the bridge.

Fig. 16, Fig. 17, and Fig. 18 show the spectra in the time-frequency plan. The sliding time-window of Joint Time Frequency Analysis [15] (JTFA) was $t_w = 20$ s.

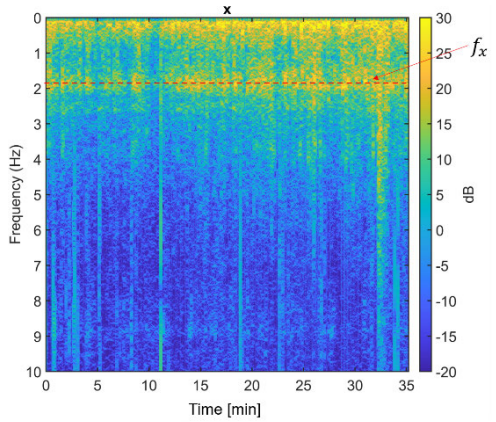

FIGURE 16. Joint Time Frequency Analysis of x-component.

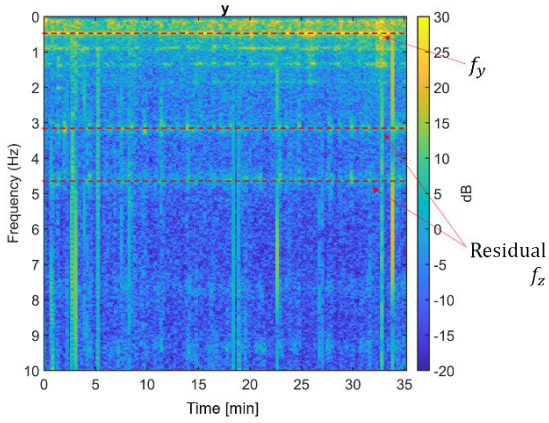

FIGURE 17. Joint Time Frequency Analysis of y-component.

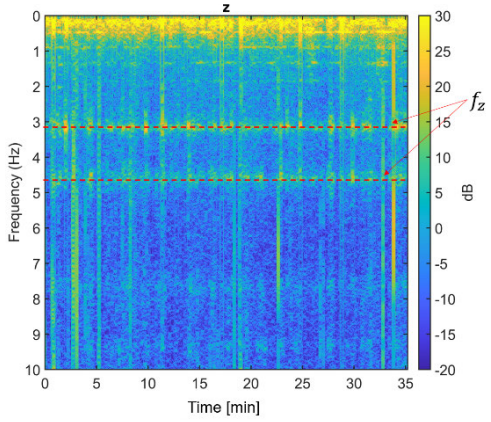

FIGURE 18. Joint Time Frequency Analysis of z-component.

The three spectra are sensitively different. Along the x-axis the main frequency is $f_x = 1.98$ Hz, along the y-axis the main frequency is $f_y = 0.50$ Hz, and along z-axis two frequencies are clearly detectable: $f_{z1} = 3.11$ Hz and $f_{z2} = 4.72$ Hz. Furthermore, we note that some residuals of z spectrum can be identified in y spectrum (Fig. 17).

VI. CONCLUSION

The paper presents a technique for retrieving the 3D displacement vector for structural monitoring using a bistatic/monostatic radar approach.

The retrieved vector uncertain was evaluated, with a simulation, considering both phase noise and positioning accuracy. The uncertain related to a possible wrong positioning of the transponder is comparable with the general experimental accuracy of the interferometric radar.

The method was validated in controlled scenario comparing the results with a seismic accelerometer.

The method was tested on a real bridge, and for the first time the 3D displacement vector was successfully detected by a radar system. The JTFA of the three components of the displacement vector has given three spectra sensitively different, as expected by structural considerations.

REFERENCES

[1] M. Pieraccini, F. Parrini, M. Fratini, C. Atzeni, P. Spinelli, and M. Micheloni, "Static and dynamic testing of bridges through microwave interferometry," *NDT E Int.*, vol. 40, no. 3, pp. 208–214, Apr. 2007.

[2] C. Gentile, "Deflection measurement on vibrating stay cables by non-contact microwave interferometer," *NDT E Int.*, vol. 43, no. 3, pp. 231–240, Apr. 2010.

[3] T. A. Stabile, A. Perrone, M. R. Gallipoli, R. Ditommaso, and F. C. Ponzo, "Dynamic survey of the musmeci bridge by joint application of ground-based microwave radar interferometry and ambient noise standard spectral ratio techniques," *IEEE Geosci. Remote Sens. Lett.*, vol. 10, no. 4, pp. 870–874, Jul. 2013.

[4] S. Placidi, A. Meta, L. Testa, and S. Rodelsperger, "Monitoring structures with FastGBSAR," in *Proc. IEEE Radar Conf.*, Johannesburg, South Africa, Oct. 2015, pp. 435–439.

[5] G. Luzi, M. Crosetto, and E. Fernández, "Radar interferometry for monitoring the vibration characteristics of buildings and civil structures: Recent case studies in Spain," *Sensors*, vol. 17, no. 4, p. 669, Mar. 2017.

[6] B. Zhang, X. Ding, C. Werner, K. Tan, B. Zhang, M. Jiang, J. Zhao, and Y. Xu, "Dynamic displacement monitoring of long-span bridges with a microwave radar interferometer," *ISPRS J. Photogramm. Remote Sens.*, vol. 138, pp. 252–264, Apr. 2018.

[7] D. Dei, D. Mecatti, and M. Pieraccini, "Static testing of a bridge using an interferometric radar: The case study of," *Sci. World J.*, vol. 2013, Dec. 2013, Art. no. 504958.

[8] A. Monti-Guarnieri, P. Falcone, D. d'Aria, and G. Giunta, "3D vibration estimation from ground-based radar," *Remote Sens.*, vol. 10, no. 11, p. 1670, Oct. 2018.

[9] Y. Deng, C. Hu, W. Tian, and Z. Zhao, "3-D deformation measurement based on three GB-MIMO radar systems: Experimental verification and accuracy analysis," *IEEE Geosci. Remote Sens. Lett.*, early access, Aug. 13, 2020, doi: 10.1109/LGRS.2020.3014342.

[10] M. Pieraccini, L. Miccinesi, and N. Rojhani, "A GBSAR operating in monostatic and bistatic modalities for retrieving the displacement vector," *IEEE Geosci. Remote Sens. Lett.*, vol. 14, no. 9, pp. 1494–1498, Sep. 2017.

[11] L. Miccinesi and M. Pieraccini, "Monostatic/Bistatic interferometric radar for monitoring slander structures," in *Proc. IEEE Conf. Antenna Meas. Appl. (CAMA)*, Bali, IN, USA, Oct. 2019, pp. 23–25.

[12] M. Pieraccini, M. Fratini, F. Parrini, C. Atzeni, and G. Bartoli, "Interferometric radar vs. Accelerometer for dynamic monitoring of large structures: An experimental comparison," *NDT E Int.*, vol. 41, no. 4, pp. 258–264, Jun. 2008.

[13] F. Viviani, A. Michelini, L. Mayer, and F. Conni, "IBIS-ArcSAR: An innovative ground-based SAR system for slope monitoring," in *Proc. IEEE Int. Geosci. Remote Sens. Symp.*, Valencia, Spain, Jul. 2018, pp. 1348–1351.

[14] M. Pieraccini and L. Miccinesi, "ArcSAR: Theory, simulations, and experimental verification," *IEEE Trans. Microw. Theory Techn.*, vol. 65, no. 1, pp. 293–301, Jan. 2017.

[15] S. Qian and D. Chen, "Joint time-frequency analysis," *IEEE Signal Process. Mag.*, vol. 16, no. 2, pp. 52–67, Mar. 1999, doi: 10.1109/79.752051.

LAPO MICCINESI (Member, IEEE) was born in Florence, Italy, in 1988. He received the B.S. degree in physics, the M.S. degree in physics of particles, and the Ph.D. degree in information engineering from the University of Florence, Florence, Italy, in 2011, 2016, and 2020, respectively.

He is currently a Post-Degree Grant Recipient with the Department of Information Engineering, University of Florence. His research interests include ground penetrating radar, radar interferometry, ground-based radar, and ground-based synthetic aperture radar.

MASSIMILIANO PIERACCINI (Member, IEEE) received the M.S. degree in physics and the Ph.D. degree in non-destructive testing from the University of Florence, Firenze, Italy, in 1994 and 1998, respectively.

From 1997 to 2005, he was a Research Assistant with the Department of Electronics and Telecommunications (former Department of Electronic Engineering), University of Florence. Since 2005, he has been an Associate Professor with the Department of Electronics and Telecommunications (now Department of Information Engineering), University of Florence. He is the author of three books, more than 160 articles, and more than nine patented inventions. His research interests include ground penetrating radar, ground-based synthetic aperture radar, interferometric radar, and microwave sensors.